Analytical Sciences (2022) 38:907–912
https://doi.org/10.1007/s44211-022-00111-9

ORIGINAL PAPER

Inhibition of direct-electron-transfer-type bioelectrocatalysis of bilirubin oxidase by silver ions

Taiki Makizuka[1] · Keisei Sowa[1] · Osamu Shirai[1] · Yuki Kitazumi[1]

Received: 18 January 2022 / Accepted: 23 March 2022 / Published online: 18 April 2022
© The Author(s), under exclusive licence to The Japan Society for Analytical Chemistry 2022

Abstract

In enzyme-based biosensors, Ag^+ eluted from the reference electrode inhibits the enzyme activity. Herein, to suppress the inhibition of bilirubin oxidase (BOD) by Ag^+, kinetic analysis was used to examine the effect of Ag^+ on the activity of BOD. It was confirmed that the addition of Ag^+ decreased the bioelectrocatalytic activity of BOD. Atomic absorption spectroscopy (AAS) suggested that Ag^+ was attached to BOD. Moreover, the changes in the visible absorption spectra after Ag^+ addition showed that Ag^+ was bound to the type I Cu sites in BOD. During oxygen reduction by BOD, the direct-electron-transfer-type bioelectrocatalytic current decreased after Ag^+ was added. The decay of the catalytic current was evaluated using kinetic analysis (assuming a pseudo-first-order reaction). Based on the analysis, the inhibition of BOD was suppressed when the Ag^+ concentration was below 0.1 μM. Referring to the solubility product of AgCl, Cl^- at a concentration of 1 mM suppressed the inhibition of the enzymatic activity by 95%.

Keywords Redox enzyme · Type I copper · Oxygen reduction · Amperometric biosensor · Silver · Silver-chloride electrode

Introduction

Bioelectrocatalysis is the coupling reaction of biocatalytic (involving redox enzymes) and electrode reactions via substrate regeneration. Direct-electron-transfer (DET)-type bioelectrocatalysis involves the direct interaction between enzymes and an electrode. DET-type bioelectrocatalysis imparts enzymatic characteristics to the electrode, creating simple systems with low energy loss [1–4]. The catalytic current by DET-type bioelectrocatalysis directly reflects the activity of the enzyme. The high substrate specificity of bioelectrocatalysis facilitates the targeted oxidation or reduction of an analyte in a sample. Therefore, the current or charge developed during bioelectrocatalysis can be used to quantify the analyte; essentially, these bioelectrocatalytic devices are electrochemical biosensors. Biosensors offer the advantages of high sensitivity, high selectivity, and ease of measurement under mild conditions. Furthermore, electrochemical biosensors have been employed in various practical applications, such as blood-glucose sensors [5, 6].

Similar to typical electrochemical systems, electrochemical biosensors also require reference electrodes. In these biosensors, Ag|AgCl|sat. KCl electrodes are often used as reference electrodes because of their stability, safety, reproducibility, and reversibility. Practically, it is important to reduce the sample volume in biosensors in order to reduce the size of the sensor. However, a small volume of sample solution can prevent the use of a salt bridge. Therefore, the reference electrode in biosensors is often directly inserted into the sample solution. In electrochemical biosensors, the eluate from the reference electrode, such as Ag^+, is expected to have a large effect on the working electrode. For example, a previous report demonstrated that eluates from the Ag|AgCl ink-printed electrodes attenuated the activity of the enzymes, thus degrading the sensor performance [7]. However, the kinetics of denaturation of enzymes by Ag^+ has not been clarified.

In this study, bilirubin oxidase (BOD) is used as a model enzyme to focus on oxygen reduction during bioelectrocatalysis. The active sites in BOD consist of four copper atoms, which can be classified into three types: type I (T1), type II (T2), and type III (T3). Additionally, BOD exhibits high DET-type catalytic activity [8]. During the DET-type

✉ Yuki Kitazumi
kitazumi.yuki.7u@kyoto-u.ac.jp

[1] Division of Applied Life Sciences, Graduate School of Agriculture, Kyoto University, Kitashirakawa Oiwake-cho, Sakyo, Kyoto 606-8502, Japan

reaction, the T1 Cu site likely functions as the electrode reaction site and the T2/T3 Cu site is the active center of the enzymatic reaction [9–11]. Attempts have been made to exploit the DET-type bioelectrocatalysis of BOD in microelectrodes for biosensing of oxygen [12–14]. The catalytic current due to the DET-type bioelectrocatalysis of BOD enables to monitor the activity of BOD adsorbed at the electrode surface. To suppress the inhibition of BOD by Ag^+, kinetic analysis is used herein to examine the effect of Ag^+ on the activity of BOD to clarify the effect of eluates from the reference electrode on the biosensor.

Experimental

Reagents and chemicals

BOD (EC 1.3.3.5) from *Myrothecium verrucaria* was purchased from Amano Enzyme, Inc. (Japan) and used without further purification. Ketjen Black (KB EC300J, Brunauer-Emmmett-Teller (BET) area of 800 $m^2\ g^{-1}$, and primary particle size of 40 nm) was purchased from Lion Corp., Japan. Poly(1,1,2,2-tetrafluoroethylene) (PTFE, 6-J) fine powder was purchased from DuPont-Mitsui Fluorochemicals Co., Ltd. (Japan). 2,2′-Azinobis(3-ethylbenzothiazoline-6-sulfonate) (ABTS) was purchased from F. Hoffmann-La Roche, Ltd. (Switzerland). Other chemicals were obtained from FUJIFILM Wako Pure Chemical Corp. (Osaka, Japan). All chemicals used in this study were of analytical grade, and all the solutions/suspensions were prepared with ultrapure water.

Determination of Cu and Ag in enzyme solution

A solution of $AgNO_3$ was added to a 5 mL of BOD solution [25 mg mL^{-1} ($L = dm^3$), BOD-1] to give a final Ag^+ concentration of 2 mM. Dialysis by using a dialysis membrane (Spectra/Por®, MWCO = 6000–8000) was then performed for two days against Ag^+-free buffer to remove free Ag^+ from the solution. To remove the aggregates formed during dialysis, the solution was centrifuged at 10,000 × g for 10 min. The supernatant was ultrafiltered using a 100 kDa Amicon® Ultra (Merck, Germany) instrument at 3000 × g for 10 min to obtain a fraction below 100 kDa. A 10 kDa Amicon® Ultra instrument was used for ultrafiltration to concentrate and separate the fractions above 10 kDa from those below 10 kDa. The fraction containing 10–100 kDa (BOD-2) was dried, the residues were dissolved in 25 mL of HNO_3 (0.1 M). A flame atomic absorption spectrophotometer (AA-7000, Shimadzu Co., Ltd., Japan) was used to determine the concentrations of Ag and Cu.

Spectrophotometric measurements

A spectrophotometer (UV1900i, Shimadzu Co., Ltd., Japan) was used to perform spectrophotometric measurements. The solution activity of BOD was determined by the increase in the concentration of $ABTS^+$ after BOD was added to the buffer solution containing ABTS and excess oxygen. The $ABTS^+$ concentration was determined from the absorption coefficient of 36,000 $M^{-1}\ cm^{-1}$ at an absorbance of 420 nm [15]. The concentration of BOD was determined from the absorption coefficient of 5000 $M^{-1}\ cm^{-1}$ at an absorbance of 600 nm [16].

Preparation of electrodes

To prepare the KB slurry, KB (40 mg) was mixed with PTFE powder (20 mg) and homogenized in 2-propanol (3.5 mL) for 2 min at 0 °C. The KB slurry (3 µL) was applied to a 3 mm (diameter) glassy carbon electrode (GCE; BAS, Japan), which was then dried to prepare the KB/GCE. The BOD solution (20 µL; 0.06 mM) in MES buffer (0.1 M; pH 7.0) was cast onto the KB/GCE surface. The prepared electrode (BOD/KB/GCE) was left for 90 min at 4 °C. MES buffer (0.1 M; pH 7.0) was used to wash excess enzyme from the electrode surface prior to the electrochemical measurements.

Electrochemical measurements

All electrochemical measurements were performed at 25 °C with an electrochemical analyzer (ALS 714C, BAS Inc., Japan) and a rotating disk electrode (RRDE-3A, BAS Inc., Japan) at a rotating speed of 4000 rpm. A platinum wire and a homemade Ag|AgCl|sat. KCl electrode were used as the counter and reference electrodes, respectively. All potentials quoted versus the reference electrode. The amperometric measurements were performed at an applied potential of 0 V.

Inhibition of the bioelectrocatalysis with AgCl was examined by adding 50 mg AgCl powder to 10 mL of the measurement solution under stirring.

Results and discussion

Binding of Ag^+ to BOD

The binding of the Ag^+ to BOD was quantified from the concentrations of Cu and Ag in the BOD solution using atomic absorption spectrometry. Table 1 lists the estimated concentrations of Ag and Cu in each sample. The results show that the BOD-1 fraction contained Cu; however, there was no

Table 1 Concentration of Ag and Cu in each enzymatic solution

	BOD-1	BOD-2
c_{Ag}/μM	−1 ± 2	7.4 ± 0.7
c_{Cu}/μM	180 ± 30	7 ± 2

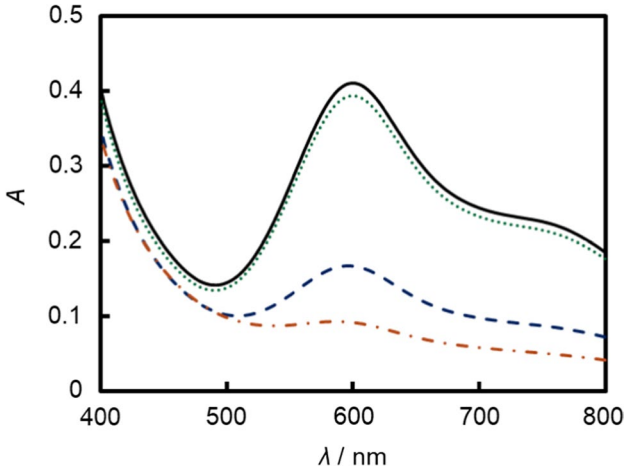

Fig. 1 Absorption spectra of BOD solutions with various concentrations of Ag^+ [0.0 (solid line), 0.1 (dotted line), 1.0 (dashed line), and 2.0 mM (dash-dotted line), respectively]

Ag. Most parts of BOD were aggregated by the addition of Ag^+ and removed by dialysis. The BOD-2 fraction, which is 10–100 kDa, likely contained Ag^+-bound BOD because its molecular mass is 61 kDa (PDB:2XLL) [17]. BOD molecule contains four copper atoms. Assuming that the Cu atoms remain in Ag^+ treated BOD, the ratio of Ag to Cu in the BOD-2 fraction indicates that approximately four Ag atoms were attached to each BOD molecule.

To determine the binding site of Ag^+, spectroscopic investigations of inactivated BOD were performed, which involved examining the effect of Ag^+ on the visible absorption spectra of the BOD solutions. Figure 1 shows the visible absorption spectra 24 h after adding $AgNO_3$ to the BOD solution (0.08 mM) at Ag^+ concentrations (c_{Ag}) of 0.0, 0.1 1.0, and 2.0 mM. In many cases where enzymes are inhibited by Ag^+, it is confirmed that Ag^+ attacks cysteine [18–20]. BOD has only one cysteine residue. The residue is strongly coordinated with the T1 Cu [21, 22]. Therefore, we hypothesized that the binding of Ag^+ to the cysteine residue would affect the T1 Cu site. Charge transfer from the cysteine-derived S atom to the T1 Cu site in BOD results in a strong absorption near 600 nm [9, 16, 23]. The absorption band at 600 nm from the coordination of cysteine to T1 Cu disappeared at high Ag^+ concentrations. Additionally, the inhibition of copper enzymes often involves the substitution of Cu^+ in the catalytic site by Ag^+ because of the analogous behavior of these two ions [24–26]. Table 2 lists the BOD activity with the addition of various Ag^+ solutions,

Table 2 Change in BOD activity after 24 h following the addition of Ag^+ solution

c_{Ag}	0 mM	0.1 mM	1 mM	2 mM
Activity change (%)	101 ± 8	110 ± 10	13 ± 3	5 ± 1

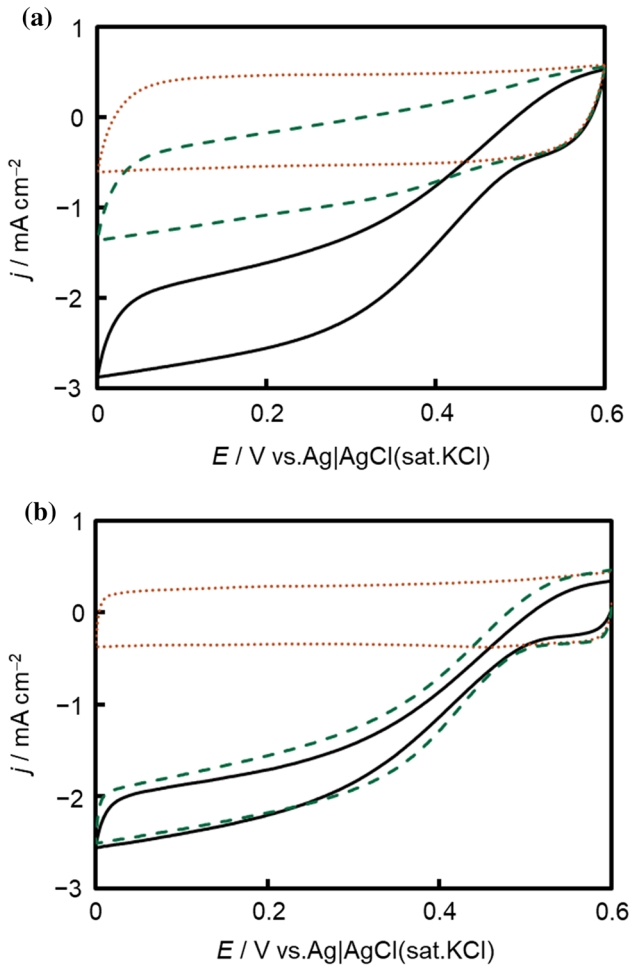

Fig. 2 CVs for the reduction of O_2 at the BOD-modified electrodes in 0.1 M MES buffer (pH 7.0) at 25 °C under O_2 atmosphere in the absence (solid line) and presence (dashed line) of (A) 50 μM $AgNO_3$ or (B) 50 μM KNO_3 at the scan rate of 20 mV s^{-1}. The dotted line shows the voltammogram recorded under Ar atmosphere

demonstrating that the inhibition of T1 Cu decreased the enzymatic activity. Therefore, the binding of Ag^+ to the T1 Cu site is a significant step in inhibiting BOD.

Inhibition of BOD during DET-type bioelectrocatalysis

Figure 2 shows the cyclic voltammograms (CVs) of the BOD/KB/GCE. In the absence of Ag^+, a current was generated from

the four-electron reduction of O_2 during the DET-type bioelectrocatalysis with BOD. The catalytic current density decreased significantly when $AgNO_3$ (50 μM) was added (Fig. 2A). Because the addition of KNO_3 did not decrease the catalytic current density (Fig. 2B), this observation suggests that Ag^+ reduced the DET-type bioelectrocatalytic activity of BOD. Figure 3 shows the decay of the catalytic current density generated from O_2 reduction at the BOD/KB/GCE after $AgNO_3$ was added. The black circles, green squares, blue diamonds, and red triangles in Fig. 3, respectively, correspond to $c_{Ag}=0$, 2, 5, and 10 μM. The current densities were normalized to the current density at $t=0$ when $AgNO_3$ was added to the electrolytic cell (j_{max}). The decrease in the current densities became more pronounced as the Ag^+ concentration increased.

Under steady-state limiting current conditions, DET-type bioelectrocatalysis comprises two steps: substrate diffusion and enzymatic reaction. However, this experiment was not strictly performed under steady-state limiting current conditions because the current density is time-dependent. However, because it took several hundred seconds for the current density to decrease, while the two-step reaction ended immediately, steady-state conditions can be considered in determining the limiting current densities. The characteristics of the two steps can be expressed by the Koutecký-Levich equation as follows [27]:

$$\frac{1}{j}=\frac{1}{j_{mt}}+\frac{1}{j_{cat}}. \tag{1}$$

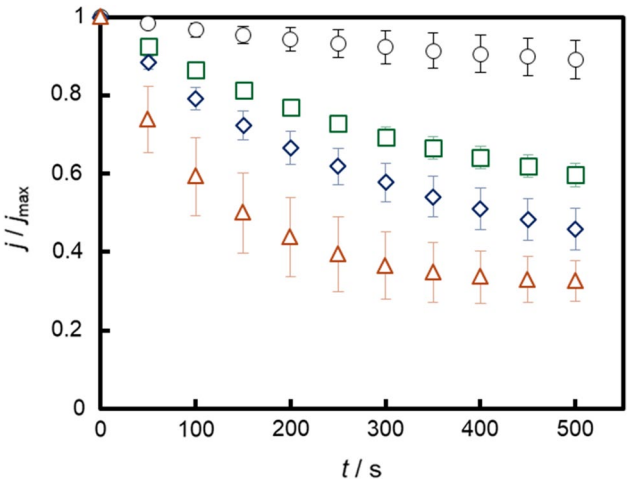

Fig. 3 Effect of Ag^+ on the normalized O_2 reduction current density at BOD-modified electrodes in 0.1 M MES buffer (pH 7.0) at 25 °C in O_2 atmosphere at 0 V with various Ag^+ concentrations (0.0 (circles), 2.0 (squares), 5.0 (diamonds), and 10.0 μM (triangles), respectively). The error bars were evaluated from student's *t*-distribution at the 90% confidence level

Here, j is the measured current density, and j_{mt} is the diffusion-controlled current density of the rotating disk electrode, which can be determined from Eq. (2).

$$j_{mt}=-0.62n_{O_2}FD_{O_2}^{2/3}\nu^{-1/6}c_{O_2}\omega^{1/2}. \tag{2}$$

The term j_{cat} is the catalytic kinetic-controlled current density, which can be determined from Eq. (3).

$$j_{cat}=-n_{O_2}Fk_{cat}\Gamma_{eff}. \tag{3}$$

Here, n_{O_2}, F, D_{O_2}, ν, c_{O_2}, k_{cat}, and Γ_{eff} are the number of electrons involved in O_2 reduction, the Faraday constant, the diffusion coefficient of O_2, the kinematic viscosity of water, the concentration of dissolved O_2, the catalytic constant of the enzyme, and the surface concentration of the effective enzyme immobilized on the electrode, respectively. Note here that k_{cat} is not equal to the catalytic constant of the enzyme in solution. It was estimated that $j_{mt}=-8.4$ mA cm^{-2} at $\omega=4000$ rpm and at 25 °C by using the following parameters: $n_{O_2}=4$, $D_{O_2}=1.7\times10^{-5}$ cm^2 s^{-1},$\nu=0.01$ cm^2 s^{-1}, and $c_{O_2}=1.2$ mM [28]. Assuming that the inhibition of BOD is slower than substrate diffusion and the enzymatic reaction, k_{cat} can be used to quantify the inhibition of BOD.

Unfortunately, BOD desorption from the electrode surface is non-negligible (black circles in Fig. 3; that is, Γ_{eff} is time-dependent. To eliminate the effect of enzyme desorption, the normalized current ratio (J_{norm}) can be determined from Eq. (4).

$$J_{norm}=\left(\frac{j_{cat,i}}{j_{cat,i,max}}\right)/\left(\frac{j_{cat}}{j_{cat,max}}\right). \tag{4}$$

Here, $j_{cat,i}$, $j_{cat,i,max}$, j_{cat}, and $j_{cat,max}$ are the catalytic current densities at t, $t=0$, in the absence of $AgNO_3$ at t, and in the absence of $AgNO_3$ at $t=0$, respectively.

From the previous discussion on the effect of Ag^+ on the inhibition of BOD, the model considers that BOD is inactivated when it binds to Ag^+ at the T1 Cu site, as shown in Eq. (5).

$$\text{BOD(active)}+Ag^+\xrightarrow{k_2}\text{BOD(inactive)} \tag{5}$$

Here, k_2 is the second-order reaction rate constant. Because the total amount of Ag^+ in the system is expected to be much larger than the amount of BOD on the electrode, pseudo-first-order conditions were adapted, based on Eq. (6).

$$\text{BOD(active)}\xrightarrow{k_1'}\text{BOD(inactive)}. \tag{6}$$

Therefore, the reaction rate can be determined from Eq. (7).

$$-\frac{d\Gamma_{eff}}{dt} = k_1'\Gamma_{eff}. \quad (7)$$

Here, $k_1'\left(\equiv k_2 c_{Ag}\right)$ is the pseudo-first-order reaction rate constant. The decay equation is derived by substituting Eq. (3) into Eq. (7), as shown in Eq. (8).

$$j_{cat}/j_{cat,max} = \exp\left(-k_1' t\right). \quad (8)$$

Using k_1' as an adjustable parameter, Eq. (8) was fitted to the time-course of the normalized catalytic current densities (J_{norm}) from 0 to 100 s; the fit was achieved with non-linear regression analysis in Gnuplot®. The best-fit curves are shown as dotted lines in Fig. 4. The fitting results agreed with the experimental results. Figure 5 shows the c_{Ag} dependence of k_1'. The linear relationship between c_{Ag} and k_1' shows that the current model explains the inhibition of BOD by Ag^+. The estimated value of k_2 from the slope is $0.00071 \pm 0.00009\ \mu M^{-1}\ s^{-1}$ [90% confidence level ($n = 14$)]. Therefore, the model can be used to predict the relationship between k_1' and c_{Ag}.

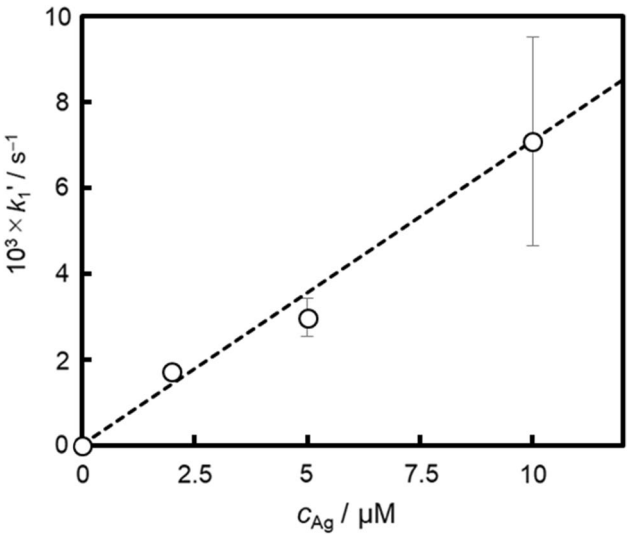

Fig. 5 Determined kinetic constants for the inhibition of BOD with Ag^+. The error bars were evaluated from student's *t*-distribution at the 90% confidence level. The dashed line shows the best-fitted regression line

Protective method for bioelectrocatalytic detection

The possibility of reducing the concentration of Ag^+ in solution by utilizing the ability of Ag^+ to form insoluble salts with various anions to suppress the inhibition reaction was investigated. The determined relationship between k_1' and the Ag^+ concentration suggests that at an Ag^+ concentration of 0.1 μM, the decay of J_{norm} after 500 s is expected to be less than 5%. Because the solubility product of AgCl is $10^{-9.76}$ (25 °C) [29], the Ag^+ concentration can be controlled to about 10^{-7} M (= 0.1 μM) in the presence of 1 mM Cl^- in the electrolyte solution. To mimic the contact of the Ag|AgCl electrode with the measurement solution, AgCl powder was added to the measurement solution. The triangles in Fig. 6 show the time-course of J_{norm} after AgCl was added. Figure 6 also shows that there was a gradual decrease in the catalytic current density and the decay of J_{norm} at 500 s was 63 ± 7%. This result suggests that the elution of AgCl from

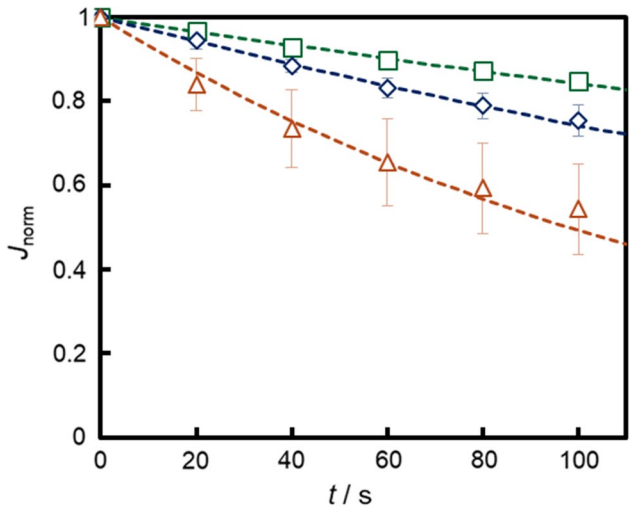

Fig. 4 Time-course of normalized catalytic current and best-fit curves estimated by non-linear regression analysis based on Eq. (8). Ag^+ concentrations of 2.0 (squares), 5.0 (diamonds), and 10.0 μM (triangles) were, respectively, used. The error bars were evaluated from student's *t*-distribution at the 90% confidence level

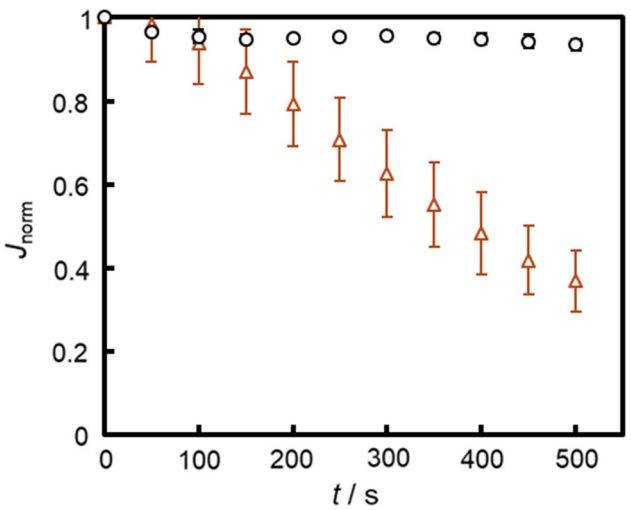

Fig. 6 Time-course of the normalized catalytic currents. Triangles and circles show the current in the buffers with AgCl (50 mg) and KCl (1 mM), respectively. The error bars were evaluated from student's *t*-distribution at the 90% confidence level

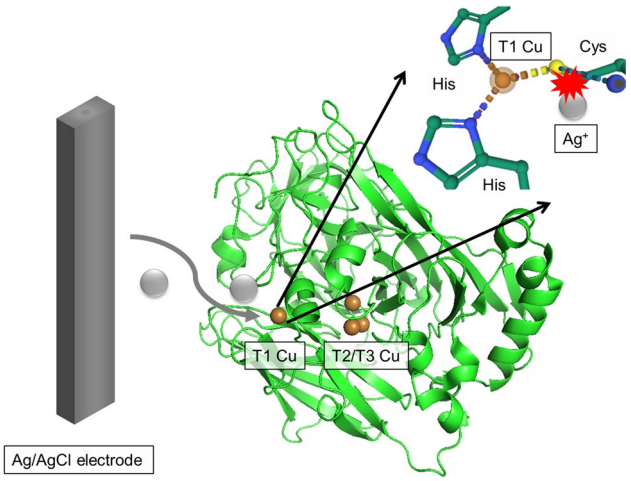

Fig. 7 Schematic image of BOD inhibited by Ag^+ dissolved from Ag/AgCl electrode

the reference electrode will reduce the functionality of the biosensor.

The circles in Fig. 6 show the J_{norm} values after AgCl was added to the buffer solution with KCl (1 mM); the decay of J_{norm} at 500 s is suppressed to $6 \pm 1\%$, which is consistent with the expectation from the kinetic analysis. Therefore, the preparation of insoluble silver salts in electrolytic solutions can protect biosensors from the negative effects of eluted Ag^+. Implicitly, these results suggest that Cl^- in biofluids likely act as a protective agent in biosensing.

Conclusion

Electrochemical methods confirmed that Ag^+ dissolved from AgCl inhibited the activity of BOD. The spectroscopic study showed that the binding of Ag^+ to the T1 Cu site was the main factor inhibiting BOD. Therefore, it is concluded that the irreversible binding of Ag^+ at the T1 Cu site inhibited BOD (Fig. 7). Kinetic analysis of the inhibition was conducted, assuming a pseudo-first-order reaction. Based on these results, the time-course of the decay of the normalized catalytic current density after 500 s is expected to be less than 5% when the Ag^+ concentration is 0.1 μM. Additionally, 1 mM KCl was successfully used to reduce the Ag^+ concentration and retard decay of the electrode during the analysis. The study reveals that to control the inhibition of BOD, the Ag^+ concentration must be reduced, which is useful knowledge for future biosensor development.

Funding This work was supported by JSPS KAKENHI (Grant Number JP21H01961).

References

1. R.S. Freire, C.A. Pessoa, L.D. Mello, L.T. Kubota, J. Braz. Chem. Soc. **14**, 230 (2003)
2. J.E. Frew, H. Allen, Eur. J. Biochem. **172**, 261 (1988)
3. Y. Kamitaka, S. Tsujimura, N. Setoyama, T. Kajino, K. Kano, Phys. Chem. Chem. Phys. **9**, 1793 (2007)
4. A.L. Ghindilis, P. Atanasov, E. Wilkins, Electroanalysis **9**, 661 (1997)
5. A. Heller, Annu. Rev. Biomed. Eng. **1**, 153 (1999)
6. A. Heller, B. Feldman, Chem. Rev. **108**, 2482 (2008)
7. Y. Matsui, Y. Kitazumi, O. Shirai, K. Kano, Anal. Sci. **34**, 1137 (2018)
8. S. Tsujimura, H. Tatsumi, J. Ogawa, S. Shimizu, K. Kano, T. Ikeda, J. Electroanal. Chem. **496**, 69 (2001)
9. T. Sakurai, K. Kataoka, Chem. Rec. **7**, 220 (2007)
10. E.I. Solomon, U.M. Sundaram, T.E. Machonkin, Chem. Rev. **96**, 2563 (1996)
11. N. Mano, L. Edembe, Biosens. Bioelectron. **50**, 478 (2013)
12. M. Miyata, Y. Kitazumi, O. Shirai, K. Kataoka, K. Kano, J. Electroanal. Chem. **860**, 113895 (2020)
13. I.S. Chang, J.K. Jang, G.C. Gil, M. Kim, H.J. Kim, B.W. Cho, B.H. Kim, Biosens. Bioelectron. **19**, 607 (2004)
14. Y. Lei, R. Sun, X. Zhang, X. Feng, L. Jiang, Adv. Mater. **28**, 1477 (2016)
15. T. Kenzom, P. Srivastava, S. Mishra, Appl. Environ. Microbiol. **80**, 7484 (2014)
16. E.I. Solomon, M.J. Baldwin, M.D. Lowery, Chem. Rev. **92**, 521 (1992)
17. J.A. Cracknell, T.P. McNamara, E.D. Lowe, C.F. Blanford, Dalton Trans. **40**, 6668 (2011)
18. H.S. Jiang, Y. Zhang, Z.W. Lu, R. Lebrun, B. Gontero, W. Li, Small **15**, 1 (2019)
19. A. Käkinen, F. Ding, P. Chen, M. Mortimer, A. Kahru, P.C. Ke, Nanotechnology **24**, 1 (2013)
20. H. Wang, X. Yang, M. Wang, M. Hu, X. Xu, A. Yan, Q. Hao, H. Li, H. Sun, Chem. Sci. **11**, 11714 (2020)
21. J.K. Ma, G.R. Bishop, V.L. Davidson, Arch. Biochem. Biophys. **444**, 27 (2005)
22. A. Shimizu, T. Sasaki, J.H. Kwon, A. Odaka, T. Satoh, N. Sakurai, T. Sakurai, S. Yamaguchi, T. Samejima, J. Biochem. **125**, 662 (1999)
23. R.H. Holm, P. Kennepohl, E.I. Solomon, Chem. Rev. **96**, 2239 (1996)
24. S.K. Singh, S.A. Roberts, S.F. McDevitt, A. Weichsel, G.F. Wildner, G.B. Grass, C. Rensing, W.R. Montfort, J. Biol. Chem. **286**, 37849 (2011)
25. M. Meury, M. Knop, F.P. Seebeck, Angew. Chem. Int. Ed. **129**, 8227 (2017)
26. F. Long, C.C. Su, M.T. Zimmermann, S.E. Boyken, K.R. Rajashankar, R.L. Jernigan, E.W. Yu, Nature **467**, 484 (2010)
27. M. Jönsson-Niedziolka, A. Kaminska, M. Opallo, Electrochim. Acta **55**, 8744 (2010)
28. Y. Miura, S. Tsujimura, S. Kurose, Y. Kamitaka, K. Kataoka, T. Sakurai, K. Kano, Fuel Cells **9**, 70 (2009)
29. C.H. Gammons, Y. Yu, Chem. Geol. **137**, 155 (1997)